THEORETICAL MODELS FOR HIGH ENERGY SOLAR FLARE EMISSIONS

Reuven Ramaty and Natalie Mandzhavidze[1]
Laboratory for High Energy Astrophysics
NASA/GSFC, Greenbelt, MD 20771

ABSTRACT

We discuss gamma ray production mechanisms and ion transport processes in solar flares. We investigate the implications of the extended GeV gamma ray emission observed from the 11 June and 15 June 1991 flares. We find that this extended emission could be produced by ions trapped in loops, provided there is a suitable combination of size, twist, field convergence and turbulent energy density. We also consider in some detail the possibility of continuous acceleration by Alfvén turbulence. We find that this would require the continuous presence of turbulence with energy density of at least 1 erg cm^{-3}. The strong pitch angle scattering caused by this turbulence leads to anisotropic pion decay emission with much steeper spectrum than observed. We discuss various alternatives, including the possibility of episodal acceleration.

I. INTRODUCTION

High energy solar flare emissions (gamma rays and neutrons) result from the interaction of flare accelerated particles with the ambient solar atmosphere. The photon and neutron production mechanisms are by now quite well understood (e.g. ref. 1). A considerable amount of research has also been carried out on the relevant particle transport processes[2-6]. New interest in these processes has been stimulated by observations of a series of X-class flares in June 1991 with instruments on the COMPTON Gamma Ray Observatory[7-9] (CGRO) and GAMMA-1 (ref. 10). Of special interest are the observations of GeV gamma ray emission that lasted for hours. These observations are raising questions on the nature of the fundamental transport processes (adiabatic motion, pitch angle scattering by plasma turbulence, drifts), as well as on the structure of the magnetic field. In addition, the possibility of particle acceleration to GeV energies over long periods of time has also been brought up. Such acceleration should take place under markedly different physical conditions than the acceleration of the ions responsible for the gamma ray emission observed during the impulsive phase of flares.

In the present paper we first review the photon production processes. We then systematically discuss the transport processes, comparing analytical approximation with Monte Carlo simulations. We investigate the very important role of plasma turbulence in both the transport and the acceleration of particles. Finally, we discuss the 11 June 1991 and 15 June 1991 flares from which extended GeV gamma ray emission was observed. We summarize the arguments in favor and against both long term trapping and continuous acceleration.

---

[1] NAS/NRC Res. Research Assoc.; also at the Inst. of Geophysics, Tbilisi, Georgia

In press: High Energy Solar Phenomena, Proc. Waterville Valley Workshop, (AIP: NY)

II. PHOTON AND NEUTRON PRODUCTION MECHANISMS

The principal mechanisms that produce high energy photons and neutrons in solar flares are summarized in Table 1. Here we briefly discuss these mechanisms and the resultant emissions.

TABLE 1, High Energy Photon and Neutron Production Mechanisms

Emissions	Processes	Observed Photons or Neutrons	Primary Ion or Electron Energy Range
Continuum	Primary Electron Bremsstrahlung	20 keV - 1 MeV >10 MeV	20keV-1GeV
Nuclear Deexcitation Lines	Accelerated Ion Interactions, e.g. ^{4}He(α,n)^{7}Be* ^{4}He(α,p)^{7}Li* ^{20}Ne(p,p')^{20}Ne* ^{12}C(p,p')^{12}C* ^{16}O(p,p')^{12}O*	Lines at e.g. 0.429 MeV 0.478 MeV 1.634 MeV 4.438 MeV 6.129 MeV	1-100 MeV/nucl
Neutron Capture Line	Neutron Production by Accelerated Ions followed by ^{1}H(n,γ)^{2}H	Line at 2.223 MeV	1-100 MeV/nucl
Positron Annihilation Radiation	β^+ Emitter or π^+ Production by Accelerated Ions, e.g. ^{12}C(p,pn)^{11}C$\rightarrow^{11}$B+e$^+$+ν p+p$\rightarrow \pi^+..,\pi^+ \rightarrow \mu^+ \rightarrow e^+$ followed by $e^+ + e^- \rightarrow 2\gamma$ $e^+ + e^- \rightarrow$ Ps+hν or $e^+ + {}^1H \rightarrow$ Ps+p Ps $\rightarrow 2\gamma, 3\gamma$	Line at 0.511 MeV Orthopositronium Continuum <511 keV	1-100 MeV/nucl
Pion Decay Radiation	π° and π^+ Production by Accelerated Particles, e.g. p+p$\rightarrow \pi^\circ, \pi^\pm$.. followed by $\pi^\circ \rightarrow 2\gamma$, $\pi^\pm \rightarrow \mu^\pm \rightarrow e^\pm$ $e^+ \rightarrow \gamma_{brem}, \gamma_{ann.\ in\ flight}$ $e^- \rightarrow \gamma_{brem}$	10MeV-3GeV	0.2-5GeV
Neutrons	Accelerated Particle Interactions, e.g. ^{4}He(p,pn)^{3}He p+p$\rightarrow \pi$+n+.. ^{22}Ne(α,n)^{25}Mg	Neutrons in Space (10-500 MeV) Neutron Induced Atmospheric Cascades (0.1-10 GeV) Neutron Decay Protons in Space (20-200 MeV)	10MeV-1GeV 0.1-10GeV 20-400MeV

Bremsstrahlung. Interactions of the accelerated electrons with ambient gas in the flare region produce continuum X-ray and gamma ray emission via nonthermal bremsstrahlung. This continuum extends from about 20 keV to over 100 MeV. At the

low energy end it merges into the thermal bremsstrahlung produced by hot flare plasma. There is no known high energy cutoff; the highest energy observed[10] bremsstrahlung is around several hundreds of MeV.

Bremsstrahlung production in solar flares in the relevant hard X-ray – gamma ray range was calculated in a thin target model yielding both angle integrated[11] and angle dependent photon spectra[12]. Both of these calculations assumed an ionized ambient gas; for the angle dependent calculation various anisotropic electron distributions were assumed. Bremsstrahlung production by ultrarelativistic electrons in flare loops, assuming that the photons are emitted along the direction of motion of the electrons, was investigated[4,13,14].

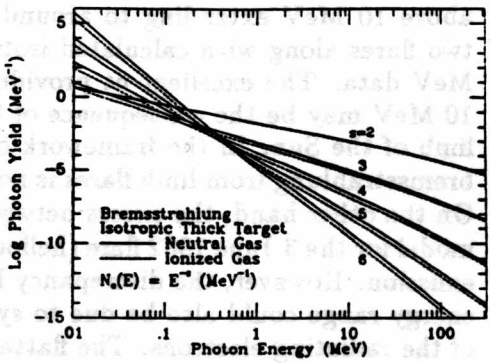

Fig. 1. Bremsstrahlung Production.

In a similar transport calculation[3] the angular distribution of the emitted radiation was also taken into account. A detailed electron transport calculation was carried out[6], however, the bremsstrahlung was only calculated[15] in an approximate manner (electron-electron bremsstrahlung was ignored), and no photon spectrum valid over a broad energy range was given.

In a previous paper[16] we presented the results of accurate calculations of angle integrated thick target bremsstrahlung in the transrelativistic region (0.3 - 1 MeV). Here we extend these calculations over a broad range of photon and electron energies (0.01 - 1000 MeV). We use the non-screened electron-proton[17] and electron-electron[18] cross sections (valid for the entire energy range), and the electron-atom cross section[19] valid in the ultrarelativistic region. Angle integrated thick target bremsstrahlung spectra, for both neutral and ionized ambient gases, are shown in Fig. 1, where the incident electron spectra are assumed to be power laws in kinetic energy. The bremsstrahlung yield in an ionized gas is generally lower than that produced in a neutral gas because of the higher rate of energy loss in the ionized case.

We have used[16] this isotropic bremsstrahlung model to fit the observed 0.3-1 MeV continuum spectra of 10 flares and 6 individual emission episodes during the 6 March 1989 flare. Although the angular distribution of the electrons could be anisotropic, the use of the isotropic model is justified since in this energy range the bremsstrahlung angular pattern is not strongly beamed and Coulomb collisions will nearly isotropize the electrons. We combined the results with data on nuclear line emission, and derived the ratio of the electron flux at 0.5 MeV to the proton flux at 10 MeV. The flux ratio of 0.5 MeV electrons to 10 MeV protons was extensively studied for solar flare particles observed in interplanetary space[20]. For these interplanetary particles, on the average, the 0.5 MeV electron to 10 MeV proton flux ratio is much larger for impulsive flares (in which particles are thought to be accelerated from hot flare plasma near the site of flare energy release) than for gradual flares (in which particles are accelerated from cooler coronal gas). The gamma ray results, pertaining to the particles which interact at the Sun, reveal an even higher electron to proton ratio, regardless of whether the flare is impulsive or gradual. This result suggests that the particles responsible for gamma ray production and the particles observed in interplanetary space from impulsive flares are probably accelerated by the same mechanism. In §III we argue that this mechanism is stochastic acceleration due to gyroresonant interactions with plasma waves.

For many flares, the gamma ray spectrum between about 1 to 8 MeV is dominated by nuclear line emission (see below). Above 10 MeV bremsstrahlung can become

important again. There are, however, only two flares (21 June 1980 and 3 June 1982) for which there are published data[21,22] on the continuum below 1 MeV and continuum above 10 MeV extending to around 100 MeV. In Fig. 2 we show the data for these two flares along with calculated isotropic bremsstrahlung spectra fitted to the 0.3 - 1 MeV data. The excellent fit provided by this model to the 21 June 1980 data above 10 MeV may be the consequence of the location of the 21 June 1980 flare close to the limb of the Sun. In the framework of standard loop geometries (§III), the directional bremsstrahlung from limb flares is not too different from the angle integrated emission. On the other hand, the excess between about 20 to 70 MeV predicted by the isotropic model for the 3 June 1982 flare (heliocentric angle 72°) could be evidence for anisotropic emission. However, the discrepancy between the data and the calculated curve in this energy range could also be due to synchrotron losses or a steepening in the spectrum of the radiating electrons. The flattening in the observed spectrum of the 3 June 1982 flare above 70 MeV is most likely due to pion decay emission discussed below.

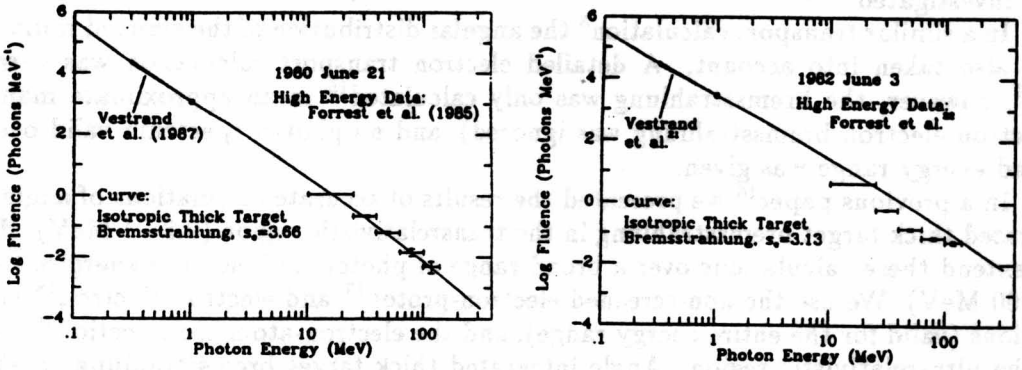

Fig. 2. Isotropic thick target bremsstrahlung fits to the 21 June 1980 and 3 June 1982 continuum.

Line Emission. Nuclear deexcitation lines result from the bombardment of ambient C and heavier nuclei by accelerated protons and α particles, and from the inverse reactions in which ambient hydrogen and helium are bombarded by accelerated carbon and heavier nuclei[23]. Because of their low relative abundances, interactions between accelerated and ambient heavy nuclei are not particularly important. Furthermore, since H and He have no bound excited states, p-p and p-He interactions can also be ignored. However, interactions of α particles with ambient He produce two strong lines, at 478 keV from ^{7}Li and at 429 keV from ^{7}Be. As the shape of the spectral feature resulting from the superposition of these α-α lines is strongly dependent on the angular distribution of the interacting α particles, measurements with good spectral resolution in the energy range 0.4 - 0.5 MeV could turn out to be particularly useful in the study of the anisotropy of the interacting particles. We return to this issue in §III.

The observed gamma ray spectrum of the 27 April 1981 flare[24] has been used to derive abundances of both the ambient gas and the accelerated particles[25]. The derived accelerated particle abundances indicate a very significant enhancement of heavy element abundances, similar to the heavy element enhancement observed in interplanetary particles from impulsive flares[26]. This supports the conclusion mentioned above that the particles responsible for gamma ray production and the particles observed in interplanetary space from impulsive flares have a common origin. The derived ambient gas composition points to enhanced Ne, Mg, Si and Fe abundances relative to C or O. The enhanced Mg, Si and Fe abundances (elements with low first ionization potential, FIP) could be understood in terms of a charge dependent ambient gas transport process from the photosphere to the chromosphere and corona which favors the collisionally

ionized, low FIP elements in the photosphere[27]. The enrichment of Ne (a high FIP element) could be due to photoionization by soft X-rays[28]. This interpretation of the Ne enhancement predicts that S should also be enhanced. Both the Ne and S enhancements have been confirmed by observations[29] with the Flat Crystal Spectrometer on SMM. Furthermore, it is possible that the feature at about 2.26 MeV observed[24] from the 27 April 1981 flare contained a significant contribution from the ^{32}S line at 2.230 MeV.

Neutrons. Neutron production in solar flares was studied in detail[5,30,31]. Solar flare neutrons have been observed directly with detectors on spacecraft, and indirectly with detectors on the ground. Solar flare neutrons have also been studied indirectly by observing neutron decay protons in interplanetary space. We have reviewed these observations[32,33]. The recent neutron observations from the June 1991 flares are summarized in Table 3 (§IV). The bulk of the neutrons which move downward to the photosphere are captured on H and ^{3}He in the photosphere. Capture on H produces the 2.223 MeV line. The ratio of the fluence in this line to the 4-7 MeV nuclear deexcitation fluence is used to determine the spectral index of the accelerated ions. We have reviewed this technique recently[16]. Studies of the 2.223 MeV line have also been used to determine the photospheric ^{3}He abundance[34].

Pion Decay Radiation. In the energy range above 10 MeV, along with the bremsstrahlung from primary electrons, there can also be a significant contribution from pion decay radiation. The theory of pion decay emission in solar flares was treated in detail[30,35] and we have reviewed the observations[32,33]. The long duration pion decay emission observed from two flares in June 1991 is discussed in §IV. We show in Fig. 3 the ratio of the angle integrated 4-7 MeV nuclear deexcitation emission[16] to the angle integrated total gamma ray production from π^o decay as a function of the proton power law spectral index S_p. Both quantities were calculated in an isotropic thick target model. The solid curve (comp 1) refers to a case in which both the ambient medium and the energetic particles have photospheric composition; the dashed curve (comp 2) refers to abundances (both of the gas and the energetic particles) derived from the gamma ray observations of the 27 April 1981 flare discussed above. We point out that, whereas $Q(4-7)$ increases by about a factor of 8 as the composition changes from comp 1 to comp 2, the pion production increases only by about 50%.

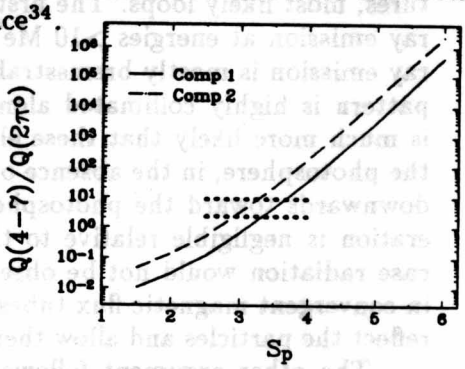

Fig. 3. Nuclear excess to pion production ratio; dots – data, see §IV.

Positrons. Positrons in solar flares result from the decay of radioactive nuclei and charged pions[36]. The contribution from radiaoctive nuclei is closely related to 4-7 MeV nuclear deexcitation emission. The ratio[37] of this positron production to the 4-7 MeV photon production is not strongly dependent on the ion spectrum and the composition. For the comp 1 abundances, it varies from 0.25 to 0.6 when the proton power law spectral index S_p varies from 5 to 3. In addition to the positron production, the 511 keV line flux also depends on the fraction of the positrons which annihilate via positronium[38] and the possible attenuation of the 511 keV line in the solar atmosphere. If the density at the annihilation site is $<10^{15}$ cm^{-3}, about 90% of the positrons will annihilate via positronium, yielding 0.65 line photons per positron. For such annihilation sites we do not expect much attenuation. If the annihilation site is deeper in the atmosphere, the number of line photons per positron increases (but

never exceeds 2); however, we also expect more attenuation, especially for flares near the limb.

Data on 511 keV line emission are available for a few flares[25,39,40] (4 and 7 August 1972, 21 June 1980, 1 July 1980, 27 April 1981, 3 June 1982). For the 21 June 1980 flare it was shown[37] that the observed[39] 511 keV line flux is consistent with that expected to accompany the observed 4-7 MeV nuclear deexcitation emission. The bulk of the positrons responsible for the 511 keV line emission in this flare resulted from the decay of radioactive positron emitters[37]. On the other hand, in the 3 June 1982 flare, the 511 keV line emission resulted from positrons from both charged pions and radioactive positron emitters[30]. The 3 June 1982 flare is the only one for which simultaneous pion decay emission and 511 keV line observations were reported.

III. TRANSPORT AND ACCELERATION

There are two strong arguments that suggest that the bulk of the observed gamma ray emission is produced by particles accelerated and trapped in closed magnetic structures, most likely loops. The first argument pertains to relativistic electrons. Gamma ray emission at energies >10 MeV was observed from many disk flares. This gamma ray emission is mostly bremsstrahlung from ultrarelativistic electrons whose radiation pattern is highly collimated along the direction of motion of the electrons. Since it is much more likely that these electrons are accelerated in the corona rather than in the photosphere, in the absence of trapping the electrons would radiate predominantly downwards toward the photosphere because the amount of material above the acceleration is negligible relative to the radiation length of relativistic electrons. In this case radiation would not be observed from disk flares. On the other hand, mirroring in convergent magnetic flux tubes, or pitch angle scattering by plasma turbulence, can reflect the particles and allow them to radiate on their way up in the solar atmosphere.

The other argument follows from the comparison of the number of interacting particles, as derived from the gamma ray observations, with the number of escaping particles from the same flare, obtained from interplanetary observations. This comparison shows that for electrons[41,42] the ratio of escaping to interacting particles (the escape ratio) is less than 1 for all the flares that were studied. For protons, the escape ratio can be both less than or greater than 1; but it is typically less than 1 for impulsive flares[16,43], indicating that at least for these flares the bulk of the protons remain trapped at the Sun. In addition, as we show below, long term trapping of particles in loops provides a natural explanation for the observation of high energy gamma ray emission hours after the impulsive phase of the flare.

a. Transport

The loop model employed in the transport calculations[2,3,5,35] for gamma ray production in solar flares consists of a semicircular coronal segment joined to two radially aligned straight segments extending to the photosphere. In the coronal segment the magnitude of the magnetic field and gas density are constant, while in the subcoronal segments both the field and gas density increase with increasing depth. In the calculations that we discuss below we use the specific model employed in our pion production calculations[35,44]. In this model, the transition between the coronal and subcoronal segments is at 2000 km above the photosphere, and R is the radius of the semicircular coronal segment. The gas density at the photosphere is 3.7×10^{17} cm^{-3}, it decreases exponentially with scale height h_a to the transition, and has a constant value n_c in

the coronal segment. The magnetic field decreases linearly in the subcoronal segments, from B_p at the photosphere to B_c at the transition.

Adiabatic Motion. To first order, the motion of the accelerated particles throughout the loop can be described by the conservation of $(1-\mu^2)/B$, where μ is the cosine of the particle's pitch angle. Particles with large pitch angle can mirror many times before they interact or their energy falls below the gamma ray production threshold. On the other hand, the energy of particles with small pitch angles can drop below the threshold before they mirror. The cone containing the velocity vectors of these particles is defined as the loss cone.

The solid curves in Fig. 4 show the amount of matter (expressed in g cm^{-2}) encountered by a particle of initial pitch angle μ_0 traversing the distance from the top of the coronal segment to the mirror point; the dashed curves represent the grammage traversed in the subcoronal segments. In cases 1, 2 and 3 the scale height and coronal density are the same, and B_p/B_c (the mirror ratio) varies.

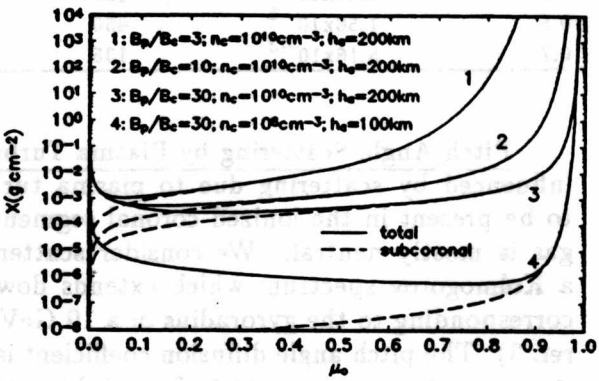

Fig. 4. Grammage from top of the loop to the mirror point.

In case 4 the mirror ratio is high, and the scale height and coronal density are low. The density at the transition is 1.7×10^{13} and 7.6×10^{8} cm^{-3} for h_a equal to 200 and 100 km, respectively. As expected, the grammage to the mirror point decreases with increasing mirror ratio (compare cases 1, 2 and 3) and decreasing scale height (compare cases 3 and 4, dashed curves). In fact, in case 4 the density just below the transition is so low that for $\mu_0 < 0.9$ essentially all of the grammage is traversed in the corona. For the other cases, the coronal contribution is important only for large pitch angles.

Using the results of Fig. 4, we can estimate, for various interaction products, the cosine μ_c of the loss-cone half-angle. For 4.438 MeV ^{12}C nuclear deexcitation photons, we assume a typical 40 MeV proton, which will fall below the threshold for line production after traversing $\sim$ 0.7 g cm^{-2}; for pion radiation, we assume a 700 MeV proton, for which the corresponding grammage is $\sim$ 50 g cm^{-2}; and for >10 MeV bremsstrahlung we take a 20 MeV electron, which will lose 10 MeV in $\sim$ 2 g cm^{-2}. Then, in case 2 for example, μ_c is approximately 0.91, 0.95, and 0.92 for 4.438 MeV line production, pion production and >10 MeV bremsstrahlung, respectively. Larger (smaller) values of μ_c will result from larger (smaller) mirror ratios. For pion production, for example, μ_c is approximately 0.81. 0.95 and 0.98 for cases 1, 2 and 3, respectively.

Particles in the loss cone will be removed from the loop on a very short time scale. In Table 2 we show the removal times for nuclear line producing and pion producing protons for three pitch angles outside the loss cones and the loop parameters of case 2. We see that the line producing protons are removed faster than the protons which produce pions. The same is true for relativistic electrons. Thus, if the motion is purely adiabatic, the pion producing protons will execute a very large number of bounces before they interact, and can, in principle, remain trapped in the loop for a long time.

TABLE 2, Time Scales, Adiabatic Motion
($B_p/B_c = 10$; $h_a = 200$ km; $n_c = 10^{10}$ cm^{-3}; $R = 10^9$ cm)

Pitch Angle Cosine	Grammage to Mirror Point (g cm^{-2})	Number of Bounces		Time (s)	
		Nuclear Lines	Pions	Nuclear Lines	Pions
0.1	$5.40\text{x}10^{-4}$	1300	$9.3\text{x}10^{4}$	$4.8\text{x}10^{3}$	$1.2\text{x}10^{5}$
0.5	$1.56\text{x}10^{-3}$	450	$3.2\text{x}10^{4}$	$3.3\text{x}10^{2}$	$8.3\text{x}10^{3}$
0.7	$5.16\text{x}10^{-3}$	135	$9.7\text{x}10^{3}$	$7.2\text{x}10^{1}$	$1.8\text{x}10^{3}$

Pitch Angle Scattering by Plasma Turbulence. The motion of the particles is also influenced by scattering due to plasma turbulence. Plasma turbulence is expected to be present in the ionized coronal segment but not below the transition where the gas is mostly neutral. We consider scattering by isotropic Alfvén turbulence with a Kolmogorov spectrum which extends down to a wave number of 3×10^{-6} cm^{-1}, corresponding to the gyroradius of a 10 GeV proton in a magnetic field of 100 G (e.g. ref. 3). The pitch angle diffusion coefficient is given by $D_{\mu\mu} = \nu\ |\mu|^{n-1}\ (1-\mu^2)$, where the scattering rate $\nu \simeq 130\ [(\gamma^2-1)^{1/3}/\gamma]\ W_A\ (\text{s}^{-1})$, W_A is the total turbulent energy density in erg cm^{-3}, γ is particle Lorentz factor, and $n = 5/3$.

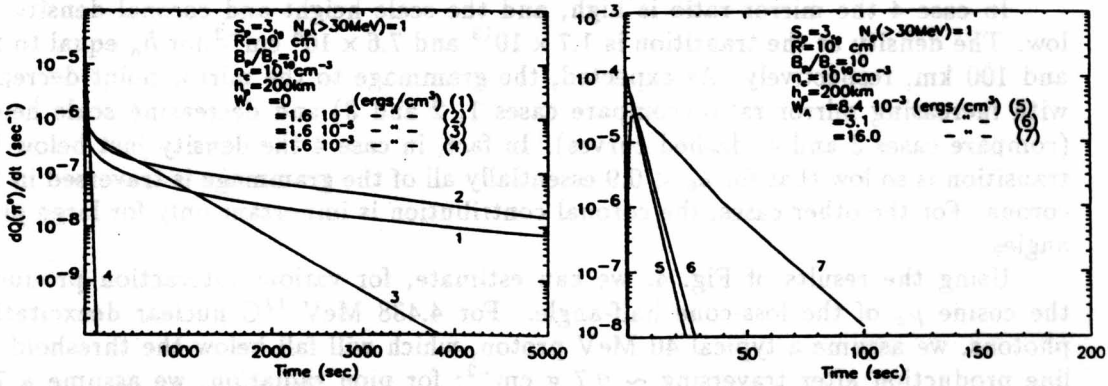

Fig. 5. Neutral pion production rate for various energy densities of plasma turbulence.

We studied the effects of the pitch angle scattering by carrying out Monte Carlo calculations of pion production. In Fig. 5 we show the time dependent rate of π^o production in the loop for various values of W_A. Curves 3 - 6 can be approximated by exponentials yielding the characteristic decay times T_d shown by-the crosses in Fig. 6. For curves 2 and 7, we estimated the decay time by using the calculations after 1000 s and 10 s, respectively. In the case of no pitch angle scattering (curve 1, $W_A = 0$) the emission decays as a power law. Also shown in Fig. 6 are analytical estimates of the dependence of T_d on W_A for 700 MeV protons (the effective energy for pion production) and the indicated loop parameters (case 2). We distinguish 3 regimes:

(i) Weak scattering. In this regime the transit time of the particles across the loop is much shorter than the pitch angle diffusion time across the loss-cone half-angle, α_c, $\pi R/[v\langle\mu\rangle] << \alpha_c^2/\nu$, where $\langle\mu\rangle$ is the average pitch angle cosine in the loss cone, and v is particle velocity. It has been suggested[45,46] that in this weak regime T_d is inversely proportional to ν (or W_A). However, our Monte-Carlo calculations do not agree with the proposed normalization coefficients. We find that in the range $10^{-5} \lesssim W_A \lesssim 10^{-3}$ erg cm^{-3}, $T_d \simeq 0.01/W_A$; at lower values of W_A this approximation breaks down, most

likely because particles with relatively small pitch angles are removed from the loop by interactions with matter before they experience significant scattering due to the plasma turbulence.

(ii) Saturated Scattering. The transition to this regime occurs when $\nu \simeq \alpha_c^2\ v\langle\mu\rangle/(\pi R)$ ($W_A \simeq 0.01$ erg cm^{-3} for the indicated parameters). In this regime the decay time scale is[3] $T_d \simeq \pi R/[v\langle\mu\rangle(1-\mu_c)]$. Using the values of μ_c given above (for case 2), we obtain values of T_d of about 4.2, 2.6, and 1.3 s, for nuclear line, pion and bremsstrahlung production, respectively. It has been suggested[2,3] that saturated pitch angle scattering is responsible for the short decay times of the gamma ray time profiles in impulsive flares (e.g. 21 June 1980).

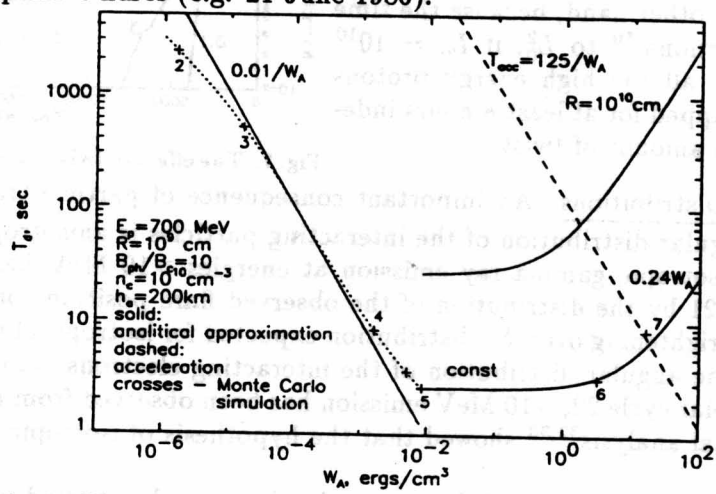

Fig. 6. Trapping and acceleration times of particles in a loop; dotted curve – guide to the eye.

(iii) Strong Scattering. In this regime the spatial diffusion time in the coronal segment is longer than the decay time in the saturated regime. To estimate the diffusive decay time we used the solution of the one dimensional diffusion equation with absorbing boundaries[47]. We found that the number of particles in the loop decays exponentially with characteristic decay time $0.81(\pi R/2)^2/2\kappa_\parallel = R^2/\kappa_\parallel$, where $\kappa_\parallel = (v^2/2\nu)/[(2-n)\ (4-n)]$ is the spatial diffusion coefficient along the filed lines[48]. Thus, the transition between the saturated and strong scattering regimes occurs when $R^2/\kappa_\parallel > \pi R/[v\langle\mu\rangle(1-\mu_c)]$. For our parameters ($R = 10^9$cm), this transition occurs at $W_A \simeq 8.7$ erg cm^{-3}. The solid curves for $W_A > 10^{-2}$ erg cm^{-3} in Fig. 6 represent the analytic decay time[46] (for two values of R),

$$T_d = \pi R/[v\langle\mu\rangle(1-\mu_c)] + R^2/\kappa_\parallel. \qquad (1)$$

This approximation, valid in the saturated and strong regimes, is in good agreement with our Monte-Carlo simulations (see Fig. 6).

Drifts. Particles can also be removed from the loop by drifts. The effects of the drifts have been studied[49] recently employing a magnetic field model that satisfies the force-free equilibrium equation, $\nabla \times \vec{B} = \lambda \vec{B}$, and boundary conditions such that the photospheric magnetic field is concentrated in two spots separated by a distance L_0. The twist exhibited by the resulting loop-like structure is determined by the parameter λ. The particles can drift to the boundaries of the loop as well as into the loss cone. The presence of twist causes some of the particles to drift on closed paths, and these particles can remain trapped in the loop indefinitely[49].

Using results from ref. 50, we plot in Fig. 7 the fraction of the particles that remain trapped in the loop as a function of time for various values of λ, $L_0 = 2 \times 10^9$ cm, and

two values of the proton energy E_p. The effects of collisions with the ambient gas and pitch angle scattering due to plasma turbulence have not been taken into account in these calculations. As expected, the low energy protons remain trapped in the loop for very long times, independent of the amount of twist.

In the absence of twist ($\lambda = 0.1$), most of the high energy protons are removed from the loop after about 1 hour. However, for $\lambda = 3.4$ (larger values lead to instabilities) a fraction (6%) of these protons remain trapped indefinitely. On the other hand, because the time scale is proportional[50] to L_0^2, if $L_0 = 10^{10}$ cm, essentially all the high energy protons will remain trapped for at least 8 hours independent of the amount of twist.

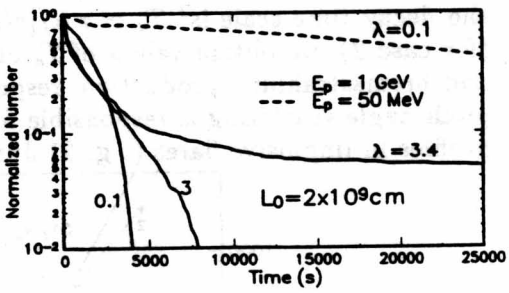

Fig. 7. The effect of twist on particle trapping.

Angular Distributions. An important consequence of particle transport in loops is that the angular distribution of the interacting particles is anisotropic[3-5,13,14]. Evidence for anisotropic gamma ray emission at energies >10 MeV has been provided in solar cycle 21 by the distribution of the observed flare positions on the Sun which showed limb brightening over the distribution expected for isotropic emission[21,51]. This implies that the angular distribution of the interacting electrons is anisotropic. However, during solar cycle 22, >10 MeV emission has been observed from many disk flares, and a statistical analysis[32,33] showed that the hypothesis of isotropic emission cannot be ruled out.

The angular distribution of the interacting ions can be studied using gamma ray line shapes[52,53]. In Fig. 8 (left panel) we show the calculated[52] profiles of the ^{7}Be and ^{7}Li lines (§II), where the arrows indicate the rest energies at 0.429 and 0.478 MeV, respectively. For no pitch angle scattering, the calculated features peak at essentially the rest energies because the angular distribution of the interacting particles peaks tangentially to the photosphere. For saturated scattering, the distribution of interacting particles is downward peaked, redshifting the lines by about 25 keV. In the right panel we show the corresponding count spectrum obtained[52] by folding the calculated spectrum (which also included the 0.511 MeV and other nuclear lines) through the SMM/GRS response. Here, the redshift is much less obvious, but still visible. For limb flares this effect is much less pronounced. Therefore, the observation of the α-α lines from 27 April 1981 flare[52] (heliocentric angle $\sim 91°$) did not allow to distinguish between saturated scattering and no scattering. On the other hand, data on the α-α lines from the 15 November 1991 disc flare (heliocentric angle 18°) obtained with YOHKOH[54] suggest the possibility of downward beaming.

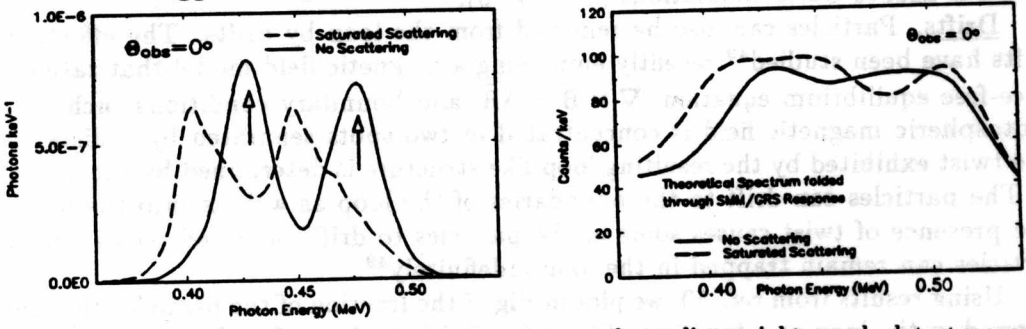

Fig. 8 (from ref. 52). Left panel: calculated spectrum of α-α lines; right panel: detector response to theoretical spectrum; θ_{obs} is heliocentric angle.

b. Acceleration

The particles are most likely accelerated in the corona. This is primarily because pitch angle scattering by plasma turbulence is required for the two most commonly discussed acceleration mechanisms, stochastic acceleration and diffusive shock acceleration[55]. There are arguments for favoring stochastic acceleration over shock acceleration in the impulsive phase of flares. At the site of the impulsive energy release, where the magnetic field is high, the Alfvén speed is expected to exceed the velocity of mass motions. In such an environment magnetoshocks will not develop, thus making shock acceleration an unlikely candidate. Furthermore, it has never been shown how shock acceleration could produce the ^{3}He and heavy element enhancements that are known to characterize both the particles observed in interplanetary space from impulsive flares, as well as the particles which produce the gamma rays. On the other hand, a credible mechanism has now been developed[56] that preferentially accelerates ^{3}He and heavy ions via gyroresonance with shear Alfvén waves. For the same reason, the observed abundance enhancements also favor stochastic acceleration over acceleration in large scale DC electric fields.

Reviews of stochastic acceleration are available in the literature (e.g. refs. 55,57). Here we limit our discussion to acceleration by gyroresonant interactions with Alfvén turbulence. As before, we assume a Kolomogorov spectrum with a cutoff at a wave number corresponding to the gyroradius of a 10 GeV proton. The average rate of energy gain of protons is given by[3] $\langle dE/dt \rangle = 1.10 \times 10^{-6}\ W_A\ V_A^2\ (\gamma^2 - 1)^{1/3}$, where $\langle dE/dt \rangle$ is in MeV s^{-1}, W_A is in erg cm^{-3}, and V_A is the Alfvén velocity in km s^{-1}. The corresponding mean acceleration time is then given by

$$T_{acc} \simeq \frac{E}{\langle dE/dt \rangle} \simeq 8.5 \times 10^8 \frac{(\gamma - 1)}{(\gamma^2 - 1)^{1/3}} \frac{1}{W_A\ V_A^2} \quad \text{s.} \qquad (2)$$

In particular, for a 700 MeV proton and V$_A$ = 2000 km/s, $T_{acc} \simeq 125/W_A$ s. This expression is plotted as a dashed line in Fig. 6.

The ratio T_d/T_{acc} determines the spectrum of the accelerated particles. For proton energies around 700 MeV, $T_d/T_{acc} \simeq 2.5\ \alpha T$, where αT is the parameter that characterizes the proton spectrum in stochastic acceleration[55]. We found[58] that the observed spectrum of the pion decay emission from the 15 June 1991 flare can be fit with $\alpha T \simeq 0.09$, where we have used relativistically correct proton spectra[59]. This implies that $T_d/T_{acc} \simeq 0.2$. The value of T_d/T_{acc} should not be much smaller, because then the spectrum is too steep to produce pions; on the other hand, the ratio should not be much larger, because then the spectrum will be much harder than the spectra derived from gamma ray observations. $T_d/T_{acc} \simeq 0.2$ requires $W_A \simeq 6$ erg cm^{-3} for $R = 10^9$ cm and $W_A \simeq 0.6$ erg cm^{-3} for $R = 10^{10}$ cm (Fig. 6). For the shorter loop, this energy density implies a short acceleration and decay time. Stochastic acceleration in relatively short loops, therefore, could play a dominant role during the impulsive phase of flares. For the longer loop, the time scales are longer, and therefore such loops are probably not adequate for impulsive phase acceleration. Concerning the extended pion decay emission observed from the 11 June and 15 June 1991 flares that lasted for hours (§IV), even for loop lengths as large as 10^{10} cm, the acceleration and decay times are still quite short (< 100 s). Thus, if we assume continuous stochastic acceleration in loops, the time profile of the emission is determined not by these times, but essentially by the injection of seed particles into the accelerator. It was suggested[60] that pion decay emission from the 3 June 1982 flare with characteristic decay time of 500 s was produced by protons stochastically accelerated during their diffusive transport

in a loop. From Fig. 6 we see that, even for a loop length of 10^{10} cm, such diffusive trapping requires $W_A \simeq 16$ erg cm^{-3}, for which T_{acc} is about 10 seconds. As discussed above, this would lead to a very hard proton spectrum, as in fact was found in ref. 60 (S_p of about 1 at relativistic energies and much flatter at lower energies). Such a spectrum is much harder than typical proton spectra derived[16,30,44,58] from gamma ray observations for both impulsive and long duration events, and is in conflict with the neutron observations[61] of the 3 June 1982 flare.

TABLE 3, High Energy Emissions from the June 1991 X-class Flares

Date	Class	Location	Max Soft X-Rays (UT)	Lines	>10 MeV Emission	π Decay Emission	Neutrons
June 4	X12	N30E70	03:39	OSSE[9] 0.51 MeV 2.22 MeV 4.44 MeV 6.13 MeV ~ 7 MeV	OSSE[9]		OSSE[9] Mt.Norikura[63,64] Neut. Mon. Neut. Telsc. Muon Telsc.
June 6	X12	N33E44	01:07	OSSE[9] 2.22 MeV 4.44 MeV 6.13 MeV ~ 7 MeV	OSSE[9]		OSSE[9]
June 9	X10	N34E04	01:43	OSSE[9] 2.22 MeV 4.44 MeV 6.13 MeV ~ 7 MeV COMPTEL[8,65] 2.22 MeV 4-7 MeV	OSSE[9]		COMPTEL[8,65]
June 11	X12	N31W17	02:09	OSSE[9] 2.22 MeV 4.44 MeV 6.13 MeV ~ 7 MeV COMPTEL[8] 2.22 MeV SIGMA[62] $F_{2.2}/F_{4-7}$	OSSE[9] EGRET[7]	EGRET[7]	
June 15	X12	N33W69	08:21	COMPTEL[8] 2.22 MeV 4-7 MeV	GAMMA-1[10]	GAMMA-1[10]	COMPTEL[8]

IV. 11 JUNE AND 15 JUNE 1991 FLARES: TRAPPING VS. CONTINUOUS ACCELERATION

Gamma ray emission was detected from the series of X-class flares that occurred in June 1991 with various instruments on CGRO[7-9], with GAMMA-1 (ref. 10) and with SIGMA/GRANAT[62]. Neutrons were also observed from 4 of these flares with CGRO and from one of them with ground level instruments[63,64] (neutron monitor,

neutron telescope and muon telescope on Mt. Norikura). In Table 3 we summarize these observations. We note, however, that for most of these data actual photon fluxes have not yet been presented.

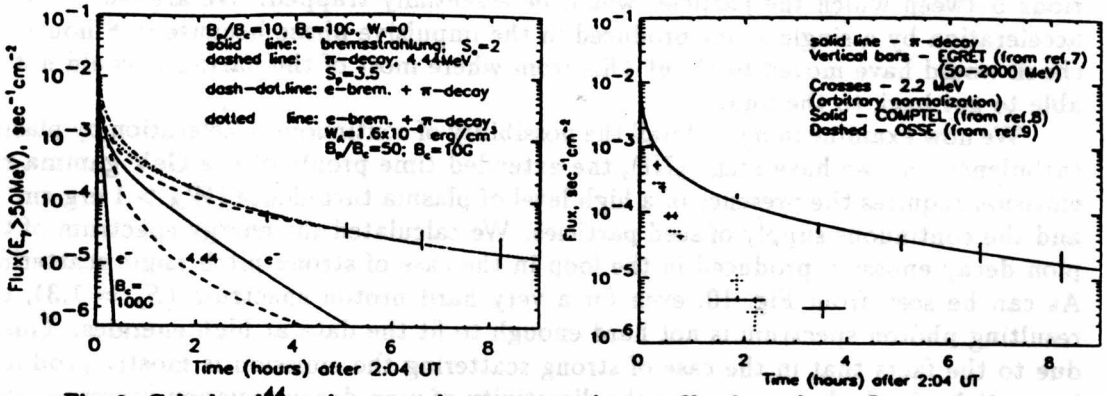

Fig. 9. Calculated[44] and measured gamma ray time profiles from the 11 June 1991 flare.

The remarkable feature of the 11 June and 15 June flares was the unusually long duration of the gamma ray emission. In the case of the 11 June flare 0.05-2 GeV gamma rays were measured with EGRET for 8 hours after the impulsive phase of the flare[7] (Fig. 9). These gamma rays are mostly of pionic origin with some admixture of primary electron bremsstrahlung at relatively low energies (50-70 MeV) during the early period of the observation (Fig. 10). Line emission at 2.22 MeV was also detected for about 2.5 hours and 4 hours following the impulsive phase, with OSSE[9] and COMPTEL[8] (Fig. 9).

Gamma rays of 0.03-3 GeV, also resulting from pion decay, were observed[10] with GAMMA-1 from the 15 June flare during two orbits of the satellite amounting to a total duration of about 2 hours. Between these two orbits 1-10 MeV emission was measured with COMPTEL[8] for about 40 minutes (Fig. 11). The central issue concerning these long lasting emissions is whether they were produced by particles that were continuously accelerated or by particles that remained trapped at the Sun after being accelerated in the impulsive phase of the flares.

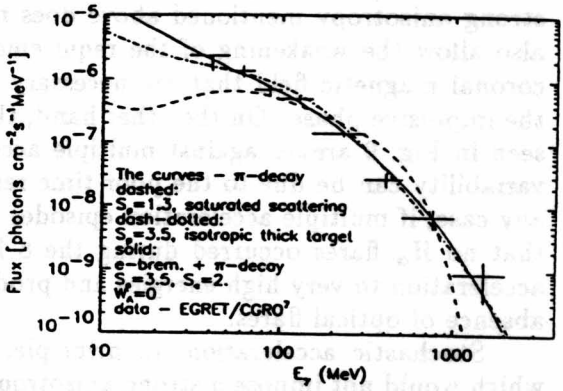

Fig. 10. Measured and calculated spectra of the gamma rays from the 11 June 1991 flare.

11 June 1991. We showed[44] that both the energy spectrum (Fig. 10) and the time profile (Fig. 9) can be fitted with the combination of primary electron bremsstrahlung and pion decay emission produced by particles trapped in coronal magnetic loops. The conditions that allow the long term trapping of the particles are: low level of plasma turbulence and relatively high mirror ratio ($W_A < 2 \times 10^{-8}$ ergs cm^{-3} for B_p/B_c=50) to prevent the fast precipitation of the particles through the loss cones; low coronal magnetic field ($B_c = 10$ G) to prevent synchrotron losses of the high energy electrons; matter density in the coronal part of the loop $n_c < 5 \times 10^{10}$ cm^{-3} to prevent Coulomb and nuclear losses. If these conditions are not satisfied, the emissions would decay too fast and therefore additional acceleration of the particles would be required.

The acceleration could be essentially continuous or episodal. Particles could be accelerated continuously by shocks moving up in the corona or by turbulence in the

loops which would have to be constantly regenerated because of the short damping time of the waves. Episodal acceleration would involve several short acceleration periods between which the particles would be essentially trapped. We argued[44] against acceleration by a single shock produced in the impulsive phase because in 8 hours the shock would have moved to about $4R_\odot$ from where most of the particles would not be able to get back to the Sun.

We now examine in more detail the possibility of continuous acceleration by plasma turbulence. As we have seen (§III), the extended time profile of the GeV gamma ray emission requires the presence of a high level of plasma turbulence ($W_A > 1$ erg cm^{-3}) and the continuous supply of seed particles. We calculated the energy spectrum of the pion decay emission produced in the loop in the case of strong pitch angle scattering. As can be seen from Fig. 10, even for a very hard proton spectrum ($S_p = 1.3$), the resulting photon spectrum is not hard enough to fit the data at high energies. This is due to the facts that in the case of strong scattering the emission is mostly produced by particles in the loss cones and the directivity of pion decay emission increases with energy. Therefore, the spectrum in the backward direction (flare heliocentric angle 35°) becomes quite steep at high energies. Thus, we conclude that during most of the EGRET observing period the level of the plasma turbulence in the loop should have been far below the saturation level. This naturally rules out the model of continuous stochastic acceleration of the particles in magnetic loops.

It may still be possible that the particles were accelerated in several episodes separated by time intervals during which the particles are mostly trapped. In this case the level of the plasma turbulence can on average be low enough so that the strong anisotropy mentioned above does not develop. In addition, this model would also allow the weakening of the requirements on the level of plasma turbulence and coronal magnetic field that are necessary if the particles are accelerated only during the impulsive phase. On the other hand, the smooth decay of the gamma ray emission seen in Fig. 9 argues against multiple acceleration episodes, although the absence of variability can be due to the poor time resolution of the gamma ray observations. In any case, if multiple acceleration episodes to GeV energies indeed took place, the fact that no H_α flares occurred during the 8 hours of EGRET observations implies that acceleration to very high energies and production of gamma rays can take place in the absence of optical flares.

Stochastic acceleration, in principle, could occur in other magnetic structures which would not impose a strong anisotropy on the interacting particles. In Fig. 10 we also show the calculated energy spectrum of pion decay emission assuming an isotropic thick target interaction model. As can be seen, the fit is reasonably good, and the fact that the measured spectrum can be explained entirely by pion decay emission without a contribution from electron bremsstrahlung makes this model even more appealing. However, the fact that the spectrum of the accelerated particles remains essentially constant for about 8 hours, while the acceleration efficiency decays by orders of magnitude, is difficult to understand within any model of continuous acceleration. The value of $S_p \simeq 3.5$, derived[62] during the impulsive phase of the flare from the fluence ratio of the 2.22 MeV and the 4.44 MeV lines, is similar to the S_p that provides the fit to the energy spectrum of the pion decay emission measured 2-8 hours later (Fig. 10).

We conclude that although continuous acceleration of the particles cannot be ruled out, the assumption of particle trapping is probably the most natural explanation of the long lasting gamma ray emission from the 11 June flare. The initially suggested[44] trapping model should be further elaborated by taking into account OSSE and COMPTEL data on nuclear line emission after these data become available in terms of actual

photon fluxes. The complete analysis should also include data on pion decay emission early in the flare when the EGRET spark chamber was saturated due to high photon fluxes. Such data can become available from OSSE and EGRET/TASC. This will allow us to constrain the parameters of the accelerated particles as well as the parameters of our model. We will also be able to check the specific predictions of particle trapping, in particular the fact that nuclear line emission should decay faster than the pion decay emission (Fig. 9). This follows from the fact that in the case of weak (or no) pitch angle scattering the spectrum of the trapped particles becomes harder with time due to Coulomb losses (§III). Of course this is only true if the effects of drifts (§III) are not significant, because the smaller Coulomb losses at high energies could be compensated by the more rapid escape from the loop due to drifts. Thus, if the comparison reveals that the nuclear lines decay faster than the pion decay emission, this would be a clear indication of particle trapping, while the absence of the effect can not be taken as an argument against trapping. As can be seen from Fig. 9, the currently available data do not allow to make such comparison because there is not sufficient overlap in time between the EGRET and OSSE/COMPTEL data, and the data are not accurate enough. One experimental fact that does provide support to trapping is the finding that, as expected in the trapping model (see Fig. 9), the electron bremsstrahlung decayed faster than the pion decay emission[7].

The other signature of trapping that could in principle allow to distinguish it from continuous acceleration is the fact that due to Coulomb losses the spectrum of the pion decay emission is expected to become harder with time (see Fig. 12b). However, as can be seen, the effect is not very strong and therefore spectral data of much higher accuracy than currently available would be necessary to verify this prediction.

15 June 1991. We studied[58] this flare by combining the GAMMA-1 pion decay emission data with the 1-10 MeV COMPTEL data. Since this range is dominated by the prompt nuclear line emission, we assume that these data also represent the time profile of the 4.44 MeV line. We obtained the absolute normalization from the measured 4-7 MeV fluence of (12.1 ± 1.9) ph/cm^2 (M. McConnell, private communication 1993) and the theoretical ratio $F_{4-7}/F_{4.4}$=3.7. The measured time profiles are shown in Fig. 11. No gamma ray observations were made during the impulsive phase of the flare because it occurred during the satellite nights of both GAMMA-1 and CGRO. In Fig. 11 we also show our fits to the GAMMA-1 and COMPTEL data which were obtained assuming that all the particles were injected into the loop instantaneously at the time of maximum of the accompanying soft X-ray emission (08^{h}21^m UT, according to GOES data). We found that to fit the GAMMA-1 data it is necessary to assume that the precipitation rate decreases with time. This can be caused, for example, by the expansion of the loop (reduction of the loss cones), or by the damping of the turbulence. The time profiles shown in Fig. 11 were calculated assuming that the energy density in the turbulence decays exponentially from an initial level of 1.6×10^{-5} ergs cm^{-3} with a characteristic time constant of 250 s. In order to simultaneously fit the time profiles of nuclear line and pion decay emissions we need a relatively low matter density in the coronal part of the loop (Fig. 11). On the time scales considered here, pion decay emission is

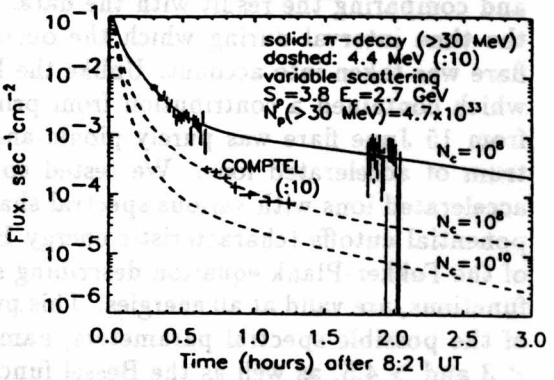

Fig. 11. Measured and calculated gamma ray fluxes for the 15 June 1991 flare[8,58].

practically insensitive to this parameter because the bulk of the pion producing ions interact in the subcoronal part of the loop. On the other hand, because of the much higher importance of the Coulomb losses, a significant fraction of nuclear lines are already produced in the corona.

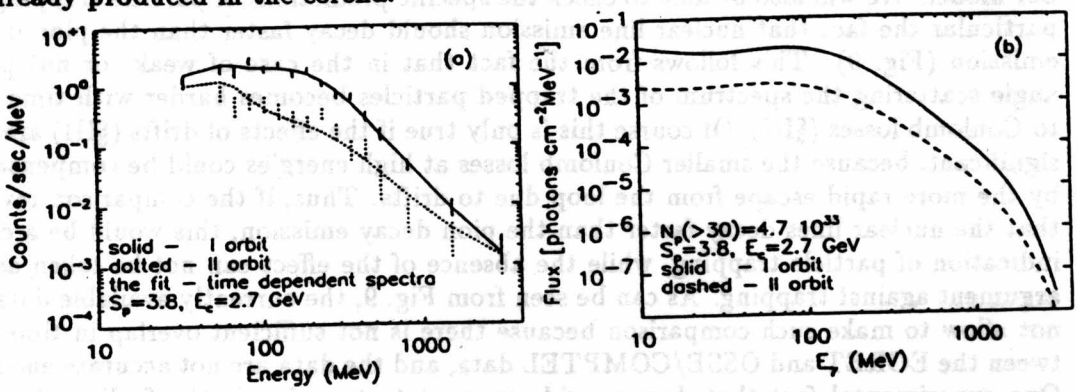

Fig. 12. Measured (GAMMA-1) and calculated energy spectra of pion decay emission from the 15 June 1991 flare (ref. 58). The fits in Fig. 12a were obtained by folding the theoretical spectra shown in Fig. 12b through the GAMMA-1 response and adding the background.

The energy spectrum of the accelerated ions used in Fig. 11 is the one that provides the best fit to the energy spectrum of the high energy gamma rays measured with GAMMA-1 (Fig. 12). We analyzed the spectral data by folding theoretical pion decay emission spectra through the GAMMA-1 response function, adding the background and comparing the result with the data. The theoretical spectra were integrated over the time interval during which the observations were made and the position of the flare was taken into account. Unlike the high energy spectrum from the 11 June flare, which contained a contribution from primary electron bremsstrahlung, the spectrum from 15 June flare was purely pionic and therefore more suitable to study the spectrum of accelerated ions. We tested spectra of pion decay emission resulting from accelerated ions with various spectral shapes, such as power laws, power laws with exponential cutoffs (characteristic energy E_c), Bessel functions and numerical solutions of the Fokker-Plank equation describing stochastic acceleration[59] which, unlike Bessel functions, are valid at all energies. This procedure allowed us to narrow down the range of the possible spectral parameters, namely we can exclude power laws with indexes < 3 and > 4.5, as well as the Bessel function. Among the remaining spectra only the power law with S_p=3.8 and E_c=2.7 GeV is consistent with GAMMA-1/COMPTEL flux ratio. However, we must note that this spectrum leads to a total time integrated 4.44 MeV flux (540 ph/cm^2) which is larger than any previously reported 4.44 MeV fluence.

The latter problem, as well as the requirement of low coronal density, can probably be overcome if instead of instantaneous injection of particles we assume that the acceleration lasted for several minutes, as in fact was indicated by neutron monitor data[66]. It is also possible that these problems are related to the simplified loop model that we are using, namely that we assume a constant magnetic field in the coronal part of the loop. In a more realistic magnetic field geometry (for example the model based on force-free equilibrium[49], §III), convergence of the magnetic field in the coronal part would allow to keep particles for a longer time in a region with a relatively low matter density, resulting in longer decay times of the nuclear line emission. Convergence of the field lines in the corona would also diminish the precipitation of the particles, and this would alleviate the problem of the very low energy density in the plasma turbulence

which we needed to postulate in order keep the particles trapped for a long time for both 11 June and 15 June flares.

Finally, we consider here also the possibility that the particles were continuously accelerated. Unlike the 11 June flare, where we could rule out continuous acceleration because the spectrum obtained in the strong scattering regime was too steep at high energies, here we can obtain a fit with such spectra. This is because the effects of the anisotropy are not very pronounced for a flare near the limb (heliocentric angle of the 15 June flare was 73°). We find that the GAMMA-1 spectral data during the first orbit can be fitted with a spectrum corresponding to a power law proton spectrum with S_p between 3.4 and 3.5 depending on the model (isotropic thick target or saturated pitch angle scattering in a loop). In both cases an exponential cutoff at 2.7 GeV is required.

On the other hand, the 15 June flare offers the possibility of comparing pion decay and nuclear line data for the same time interval, namely the 40 minute interval of the COMPTEL observations (Fig. 11). Interpolating the pion decay flux between the two GAMMA-1 orbits and integrating it over the COMPTEL observation period, we obtain $F_\gamma(\pi) = (2.1 \pm 0.5)$ ph/cm^2. The corresponding ratio $F_{4-7}/F_\gamma(\pi)$ is plotted in Fig. 3, where the theoretical curves are based on isotropic thick target calculations (§II). The possible range of the power law spectral index is 2.9-3.6, depending on the composition. This range is consistent with that obtained from the analysis of the pion decay spectrum. (Note that the spectrum of the pion decay emission practically does not depend on the composition and the ratio of the nuclear line yield to the total energy integrated pion decay emission yield does not depend much on the presence of cutoff in the primary proton spectrum above 1 GeV). We conclude that continuous acceleration cannot be ruled out for this flare.

Observations of line emission at 511 keV could help distinguish between the models. The 4-7 MeV fluence of about 12.1 photons cm^{-2} (Fig. 11) should be accompanied by a 511 keV fluence of about 3 photons cm^{-2} resulting from radioactive nuclei (using a positron to 4-7 MeV photon production ratio of 0.4, and a positronium fraction of 0.9, §II). Even in the case of strong pitch angle scattering, we do not expect much attenuation, because, similar to nuclear deexcitation lines[2], the radioactive nuclei are expected to be produced at relatively high altitudes in the solar atmosphere. In addition, we also expect 511 keV line emission from positrons resulting from π^+ decay. Using a π^+/π° production ratio[37] of 4, we obtain a 511 keV line flux of $4.3f$ photons cm^{-2}, where f takes into account the uncertainty in the positronium fraction and the attenuation. There are no calculation of this parameter for solar flare loop models. We estimate that f will be about 0.7, when there is no scattering. When there is strong scattering, the positrons are produced deep in the atmosphere[35]. Therefore, for a flare near the limb, f should be close to 0. Thus, the predicted 511 keV line fluence is between 3 and 6 photons cm^{-2}, depending on the model. We also expect that the 511 keV line will be accompanied by positronium continuum below 511 keV. The CGRO observing period (0.6-1.3 hours, Fig. 11) is particularly favorable because there should not be much primary electron bremsstrahlung during this late phase of the flare.

V. SUMMARY

We have reviewed the accelerated particle interaction and transport processes relevant to gamma ray production in solar flares. The transport processes that we considered are adiabatic motion, pitch angle scattering by plasma turbulence, spatial diffusion and drifts. These processes affect the gamma ray time profiles, angular distributions and gamma ray line shapes. We also considered stochastic acceleration by

the same turbulence that scatters the particles. We point out that, in addition to the energy density in plasma turbulence, the size of the loop in which the particles are accelerated is an important parameter that determines the energy spectrum of the particles, as well as the rise and decay times of the accompanying gamma ray emission. Flares with very impulsive time profiles (both rise and decay times on the order of seconds) require acceleration in small loops ($R \lesssim 10^9$ cm).

We investigated the long term trapping of particles in magnetic loops as a possible explanation of the extended gamma ray emission observed from the 11 June and 15 June 1991 flares. We find that such trapping requires large loops, or smaller but twisted loops, or loops which cover a large area of the solar surface. For all of these structures, the turbulent energy density should be sufficiently low to avoid the fast precipitation of particles through the loss cones. We also investigated the possibility of continuous acceleration of particles over extended time periods. The turbulent energy density required by such acceleration will cause the rapid precipitation of the particles and will lead to a highly anisotropic angular distribution of GeV gamma rays from pion decay. We found that the resultant energy spectrum is inconsistent with observations. However, we cannot rule out the possibility that particles were accelerated during several discrete episodes and remained essentially trapped between them.

The combination of nuclear deexcitation line and pion decay emissions allows us to determine, for the first time, the spectrum of the accelerated protons over a broad energy range (10 MeV-5 GeV). For the two flares mentioned above the spectrum is consistent with a power law of index around 3.5, and for one of them (15 June) there is also a high energy exponential cutoff around 3 GeV. There is as yet no convincing acceleration theory that predicts a single power in kinetic energy over this broad energy range.

We wish to acknowledge Y.-T. Lau and J. A. Miller for useful discussions, V. Akimov and N. Leikov for the collaboration in interpreting the GAMMA-1 data, and J. G. Skibo for help with the bremsstrahlung calculations.

REFERENCES

1. R. Ramaty and R. J. Murphy, Space Science Rev., 45, 213 (1987).
2. X. M. Hua, R. Ramaty and R. E. Lingenfelter, ApJ, 341, 516 (1989).
3. J. A. Miller and R. Ramaty, ApJ, 344, 973 (1989).
4. A. L. MacKinnon and J. C. Brown, Astr. and Ap., 232, 544 (1990).
5. V. G. Gueglenko et al., Solar Phys., 125, 91 (1990).
6. J. M. McTiernan and V. Petrosian, ApJ, 359, 524 (1990).
7. G. Kanbach et al., Astr. and Ap. Suppl., 97, 349 (1993).
8. J. M. Ryan et al., in: Compton Workshop (St. Louis), in press (1993).
9. R. J. Murphy et al., in: Compton Workshop (St. Louis), in press (1993).
10. V. V. Akimov et al., 22nd Internat. Cosmic Ray Conf. Papers, 3, 73 (1991).
11. T. Bai, PhD. Dissertation, Univ. of Md., (1977).
12. C. D. Dermer and R. Ramaty, ApJ, 301, 962 (1986).
13. P. E. Semukhin and G. A. Kovaltsov, 19th Internat. Cosmic Ray Conf. Papers, 4, 106 (1985).
14. V. Petrosian, ApJ, 299, 987 (1985).
15. J. M. McTiernan and V. Petrosian, ApJ, 359, 541 (1990).
16. R. Ramaty, N. Mandzhavidze, B. Kozlovsky, and J. Skibo, Adv. Space Res.(COSPAR), in press (1993).
17. H. W. Koch and J. W. Motz, Rev. Mod. Phys., 31, 920 (1959).
18. E. Haug, Zs. Naturforsch., 30a, 1099 (1975).
19. G. R. Blumenthal and R. J. Gould, Rev. Mod. Phys., 42, 237 (1970).

20. M. B. Kallenrode, E. W. Cliver, and G. Wibberenz, ApJ, 391, 370 (1992).
21. W. T. Vestrand et al., ApJ, 322, 1010 (1987).
22. D. J. Forrest et al., 19th Internat. Cosmic Ray Conf. Papers, 4, 146 (1985).
23. R. Ramaty, B. Kozlovsky, and R. E. Lingenfelter, ApJ Supp., 40, 487 (1979).
24. Murphy, R. J., G. H. Share, J. R. Letaw, and D. J. Forrest, ApJ, 358, 298 (1990).
25. R. J. Murphy, R. Ramaty, B. Kozlovsky, and D. V. Reames, ApJ, 371, 793 (1991).
26. D. V. Reames, ApJ Supp., 73, 235 (1990).
27. J.-P. Meyer, ApJ Supp., 57, 151 (1985).
28. A. Shemi, Mon. Not. Royal Astr. Soc., 251, 221 (1991).
29. J. T. Schmelz, ApJ, 408, 381 (1993).
30. R. J. Murphy, C. D. Dermer, and R. Ramaty, ApJ Supp., 63, 721 (1987).
31. X. M. Hua and R. E. Lingenfelter, Solar Phys., 107, 351 (1987).
32. N. Mandzhavidze and R. Ramaty, Nuclear Physics B, Proc. Suppl., in press (1993).
33. R. Ramaty and N. Mandzhavidze, in: Compton Workshop (St. Louis), in press (1993).
34. X. M. Hua and R. E. Lingenfelter, ApJ, 319, 555 (1987).
35. N. Mandzhavidze and R. Ramaty, ApJ, 389, 739 (1992).
36. B. Kozlovsky, R. E. Lingenfelter, and R. Ramaty, ApJ, 316, 801 (1987).
37. R. J. Murphy and R. Ramaty, Adv. Space Res., 4, No. 7, 127 (1984).
38. C. J. Crannell, G. Joyce, R. Ramaty, and C. Werntz, ApJ, 210, 582 (1976).
39. G. H. Share, E. L. Chupp, D. J. Forrest, and E. Rieger in: Positron Electron Pairs in Astrophysics, eds. M. L. Burns et al. (New York:AIP), p. 15 (1983).
40. R. Ramaty, in: The Physics of the Sun, eds. P.A. Sturrock (Reidel, Dordrecht, 1986) Vol. II, p. 291.
41. B. Klecker et al., 21st Internat. Cosmic Ray Conf. Papers, 5, 80 (1990).
42. E. I. Daibog, Yu. I. Logachev, V. G. Stolpovsky, V. F. Melnikov and T. S. Podstrigach, 21st Internat. Cosmic Ray Conf. Papers, 5, 96 (1990).
43. E. W. Cliver et al., ApJ, 343, 953 (1989).
44. N. Mandzhavidze and R. Ramaty, ApJ, 396, L111 (1992).
45. C. F. Kennel and H. E. Petschek, JGR, 71, 1 (1966).
46. V. G. Gueglenko, L. G. Kocharov, and G. A. Kovaltsov, in: Nuclear Astrophysics, ed. G. E. Kocharov (St. Petersburg), p. 62 (1991).
47. R. Ramaty in: High Energy Particles and Quanta in Astrophysics, eds. F. B. McDonald and C. E. Fichtel (MIT, Cambridge), p. 122 (1974).
48. J. A. Earl, ApJ, 193, 231 (1974).
49. Y.-T. Lau, T. G. Northrop, and J. M. Finn ApJ, in press (1993).
50. Y.-T. Lau and R. Ramaty, this volume.
51. E. Rieger, Solar Phys., 121, 323 (1989).
52. R. J. Murphy, X. M. Hua, B. Kozlovsky, and R. Ramaty, Ap.J, 351, 299 (1990).
53. C. Werntz, F. L. Lang, and Y. E. Kim, ApJ Supp., 73, 349 (1990).
54. M. Yoshimori et al., ApJ Supp., in press (1993).
55. M. A. Forman, R. Ramaty, and E.G. Zweibel, in: The Physics of the Sun, eds. P.A. Sturrock (Reidel, Dordrecht, 1986) Vol. II, p. 249.
56. J. A. Miller and A. Viñas, ApJ, in press (1993).
57. J. A. Miller and R. Ramaty, in: Particle Acceleration in Cosmic Plasmas, eds. G.P. Zank and T.K. Gaiser (AIP, New York, 1992) p. 223.
58. N. Mandzhavidze, R. Ramaty, V. Akimov, and N. Leikov, 23rd Internat. Cosmic Ray Conf. Papers, in press (1993).
59. J. A. Miller, N. Guessoum, and R. Ramaty, ApJ, 361, 701 (1990).
60. J. M. Ryan and M. A. Lee, ApJ, 368, 316 (1991).
61. E. L. Chupp et al., ApJ, 318, 913 (1987).
62. G. Trottet et al., Astr. and Ap. Suppl., 97, 337 (1993).
63. Y. Muraki et al., ApJ, 400, L75 (1992).
64. K. Takahashi et al., 22nd Internat. Cosmic Ray Conf. Papers, 3, 37 (1991).
65. J. M. Ryan et al., in: The Compton Observatory Science Workshop, p. 470 (1992).
66. V. Akimov et al., this volume.